

Article

Numerical Simulation of Natural-Gas-Hydrate Decomposition in Process of Heat-Injection Production

Qiannan Yu ¹, Huimin Tang ², Chenglong Li ³, Zhijing Chen ^{1,*}, Kun Zhang ^{1,*}, Yang Yu ¹ and Shuang Liang ⁴

¹ College of Energy and Power Engineering, Guangdong University of Petrochemical Technology, Maoming 525000, China; canaan184@163.com (Q.Y.)

² Hainan Branch CNOOC (China) Co., Ltd., Haikou 570311, China

³ Heilongjiang Key Laboratory of Reservoir Physics and Fluid Mechanics in Porous Medium, Daqing 163712, China

⁴ School of Petroleum Engineering, Northeast Petroleum University, Daqing 163318, China; liangshuang21@163.com

* Correspondence: labnglab@outlook.com (Z.C.); zkgdupt@outlook.com (K.Z.); Tel.: +86-668-2923-531 (Z.C.)

Abstract: Heat-injection production is a common technique for gas-hydrate development, and the mechanism needs further in-depth study, particularly of the decomposition characteristics of natural-gas hydrate, which are important fundamental issues. The natural gas-hydrate-reservoir model is based on a mathematical description of reservoir properties that considers the effects of hydrate decomposition and reservoir stress conditions. The aim of our investigation was to analyze the production and decomposition characteristics of natural-gas hydrates based on the results of numerical simulations of heat-injection production. The effects of different heat-injection temperatures and heat-injection rates on production were compared, and the decomposition characteristics of hydrates were evaluated qualitatively and characterized quantitatively by temperature distribution, saturation distribution, and the decomposition front in the process of heat-injection production of natural-gas hydrate. The results showed that, with the increase in the heat-injection temperature, the decomposition front moved faster, the area share of decomposition zone increased, but the increase extent decreased. The high heat-injection rate had a more significant effect than the heat-injection temperature in promoting the decomposition of natural-gas hydrate.

Keywords: natural-gas hydrate; heat-injection production; decomposition characteristics; temperature distribution; saturation distribution; decomposition front



Citation: Yu, Q.; Tang, H.; Li, C.; Chen, Z.; Zhang, K.; Yu, Y.; Liang, S. Numerical Simulation of Natural-Gas-Hydrate Decomposition in Process of Heat-Injection Production. *Processes* **2023**, *11*, 2349. <https://doi.org/10.3390/pr11082349>

Academic Editor: Vladimir S. Arutyunov

Received: 5 July 2023

Revised: 29 July 2023

Accepted: 1 August 2023

Published: 4 August 2023



Copyright: © 2023 by the authors. Licensee MDPI, Basel, Switzerland. This article is an open access article distributed under the terms and conditions of the Creative Commons Attribution (CC BY) license (<https://creativecommons.org/licenses/by/4.0/>).

1. Introduction

Natural-gas hydrate is recognized as a promising subsequent clean-energy source with the broad prospect of replacing traditional fossil energy such as oil and natural gas [1]. Natural-gas hydrate exist as a solid in reservoirs and needs to be decomposed in the process of exploration to release the natural gas. At present, the main methods for natural-gas-hydrate exploration and production at home and abroad are: heat injection [2]; pressure reduction [3]; CO₂ replacement [4]; and inhibitor injection [5]. Most production technologies for natural-gas hydrate have been proposed based on the theory of disruption of the phase-equilibrium properties. The decomposition of natural-gas hydrate is a complicated process involving heat and mass transfer and phase transitions. The feasibility of heat-injection production of natural-gas hydrate has been proved by the trial production of the Mallik hydrate reservoir in Canada [6,7], but there are still obvious drawbacks such as high heat loss and low heat-utilization rate, and the mechanism and mining process of heat-injection production of natural-gas hydrate still needs further in-depth study, particularly of the decomposition characteristics of natural-gas hydrate.

The mechanism of heat-injection production of natural-gas hydrate and its numerical simulation have been studied more extensively and some progress has been made.

McGuire (1981) proposed a thermodynamic model for thermal decomposition of natural-gas hydrate and created a flow model of heat-injection production, concluding that heat injection is a more advantageous mining method [8]. Holder and Angert (1982) developed a mathematical model for heat-injection production of natural-gas hydrate and further demonstrated its feasibility [9]. Vidyadhar and Fodhole (1985) developed a model for heat-injection production of a one-dimensional radial natural gas-hydrate reservoir considering hydrate saturation in porous media [10]. Selim et al. (1990) developed an analytical model for heat-injection production of a one-dimensional radial natural-gas-hydrate reservoir and derived an analytical solution [11]. Swinkels et al. (1999) developed a model with three-dimensional of force-finite difference considering phase equilibrium, energy conservation, and reservoir compaction [12]. Moridis et al. (2003) added the EOSHYDR2 module to the TOUCH2 simulator, which is capable of thermal energy simulations for multicomponents, to achieve equilibrium kinetic simulations of hydrate decomposition [13,14]. Tang (2006) developed a heat-transfer model for the decomposition and hydrate zones in sediment by neglecting the influence of mass transfer and the change of physical properties [15]. Du (2007) developed a kinetic model of hydrate decomposition during heat-injection production considering reformed hydrate [16]. Hou (2008) established a kinetic model of hydrate decomposition with basic equations including mass conservation and energy conservation considering reformation of hydrates [17]. Li et al. (2008) developed a one-dimensional radial mathematical model of the decomposition front of hydrate based on energy conservation, and the simulation results were in good agreement with the experimental results [18]. Phirani et al. (2009) considered five phases (hydrate, gas, liquid, salt, and ice) and four components (hydrate, methane, water, and salt) to establish a mathematical model for three-dimensional heat-injection production of hydrates [19]. Li (2010) developed a one-dimensional mathematical model based on the Selim model considering only the flow of gas [20]. Bai (2011) analyzed the extraction mechanism of heat-injection production of natural-gas-hydrate reservoirs using a three-dimensional model established by considering seepage of multi-phase and multi-component fluid, kinetic equations of hydrate decomposition, phase change of hydrate and water, and heat conduction between different components [21]. Zhao (2013) improved the one-dimensional heat-injection production model considering the heat absorption and exotherm during phase change of hydrates, and established an axisymmetric mathematical model for distribution of formation temperature during heat-injection production of natural-gas hydrate [22]. Zhao et al. (2015) developed a two-dimensional axisymmetric model to investigate the effect of heat-transfer properties of methane hydrates on hydrate decomposition characteristics [23]. Sun et al. (2017) developed a thermal–fluid–solid-coupled model for hydrate decomposition involving reservoir mechanical properties to simulate pore pressure, hydrate saturation, and reservoir physical parameters during heat-injection production [24]. Liu et al. (2018) used Fluent to extend a numerical model applicable to heat-injection production of natural-gas hydrate, and conducted a simulation analysis of heat injection and gas production [25]. Liu Y et al. (2019) carried out numerical simulations to study hydrate decomposition and production from different types of wells and optimization of heat-injection parameters, and the results showed that the production capacities of horizontal wells developed with heat injection were significantly higher than those of conventional vertical wells [26]. Peng and Xia (2020) used HydrateResSim to numerically simulate the effect of heat injection on the development of different types of gas-hydrate reservoirs, showing that heat-injection production is more efficient for the development of Class I hydrate reservoirs [27,28]. More research on EOR techniques in developing unconventional energy resources provided good lessons for heat-injection production [29,30]. Previous studies have shown that hydrate decomposition kinetics and heat transfer have relatively little influence on the results of numerical simulations, and that the spatial properties of reservoirs and gas–water flow parameters are decisive; however, most studies ignore the key issue of the evolution of gas-hydrate-reservoir properties in the process of heat-injection production. The modeling of basic parameters such as permeability and porosity and their evolution mechanisms need to be

further improved, and the lack of dynamic modeling of physical parameters limits further work on numerical simulation of process of heat-injection production of gas hydrate.

This paper describes a novel natural-gas-hydrate reservoir model based on some basic assumptions and a mathematical description of reservoir properties considering the effects of hydrate decomposition and reservoir stress conditions. A mathematical model of natural-gas-hydrate decomposition was developed by the conservation-of-mass equation, the conservation-of-energy equation, and the equation of kinetics for hydrate decomposition. Based on the results of further numerical simulations of heat-injection production of natural-gas hydrate, the production and decomposition characteristics were analyzed. The effects of different heat-injection temperatures and heat-injection rates on production were compared, and the decomposition characteristics of hydrates were evaluated qualitatively and characterized quantitatively by temperature distribution, saturation distribution, and the decomposition front in process of heat-injection production of natural-gas hydrate.

2. Numerical Simulation Modeling Section

2.1. Basis for Model of Natural-Gas-Hydrate Reservoir

2.1.1. Basic Assumptions

The mathematical modeling was based on some basic assumptions by combining the microscopic mechanism of hydrate decomposition, and the main influencing factors are highlighted below:

Considering the natural-gas-hydrate reservoir is of the same nature in all directions and the pores are uniformly distributed, natural-gas hydrates are filled in a porous medium, and properties of the porous medium and fluid remain constant.

Considering only the presence of gas, liquid, and solid phases in fluid, the gas phase is methane, the liquid phase is water, the solid phase is natural-gas hydrate, and the dissolution of methane in water is ignored.

Considering only SI natural-gas hydrate, the molecular formula of natural-gas hydrate is assumed to be $8\text{CH}_4 \cdot 46\text{H}_2\text{O}$.

Considering the gas and liquid phases flow through the porous medium and the fluid flow obeys Darcy's law.

2.1.2. Mathematical Description of Reservoir Properties

The existing numerical models for heat-injection production of natural-gas hydrate generally ignore the effect of reservoir stress conditions on reservoir properties [31–33]. The inadequacy of dynamic models of physical parameters limits further work on numerical simulation, and the effects of hydrate decomposition and reservoir stress on the basic properties of hydrate reservoirs are considered in the following mathematical description of reservoir properties.

Considering the natural-gas hydrate as part of the pores of the porous medium, and the fact that the porous medium is filled with methane gas, water, and natural-gas hydrate:

$$S_w + S_g + S_h = 1 \quad (1)$$

where S_w is saturation of water, S_g is saturation of gas, and S_h is saturation of hydrate.

$$\varphi_i = \varphi_0(1 - S_h) \quad (2)$$

where φ_i is initial porosity and φ_0 is porosity as saturation of hydrate is 0.

Considering permeability as a function of fluid porosity, permeability of the reservoir can be characterized by the Carmen–Kozeny equation:

$$K_i = K_0(1 - S_h)^{C_h} \quad (3)$$

where K_i is initial permeability of the reservoir, K_0 is permeability of the reservoir as saturation of hydrate is 0, and C_h is the empirical-fit coefficient.

The effects of heat injection on the geomechanics in natural-gas-hydrate reservoirs should be discussed [34], and the effects of hydrate decomposition and stress changes during production should be considered in a mathematical description of reservoir properties. Under the influence of thermal-fluid solid coupling of heat injection and hydrate decomposition, the effective stress of a reservoir changes greatly, and then porosity and permeability of the reservoir change accordingly [35].

$$K = K_i(a\sigma^2 + b\sigma + c) \quad (4)$$

where K is permeability of the reservoir; K_i is initial permeability of the reservoir; σ is effective stress; and a , b , and c are regression coefficients obtained from experimental tests.

$$\varphi = \varphi_i m e^{n\sigma} \quad (5)$$

where φ is porosity of the reservoir; φ_i is initial porosity of the reservoir; and, m and n are regression coefficients obtained from experimental tests.

$$\sigma = \frac{\sigma_x + \sigma_y + \sigma_z}{3} - \alpha P_a \quad (6)$$

where σ_x , σ_y , and σ_z are principal stresses in the x , y , z direction, α is the Biot coefficient, and P_a is atmospheric pressure [36].

Considering the effects of hydrate decomposition and stress changes during production, porosity and permeability of the reservoir can be depicted as:

$$K = K_0(a\sigma^2 + b\sigma + c)(1 - S_h)^{C_h} \quad (7)$$

$$\varphi = \varphi_i(1 - S_h)m e^{n\sigma} \quad (8)$$

Considering capillary pressure in the pores of porous media as a function of the saturation of water and gas, capillary pressure can be characterized by the Van Genuchten capillary-pressure equation.

$$P_c = -P_a \left(\left(\frac{S_w - S_{rw}}{1 - S_{rw}} \right)^{-1/\lambda_c} - 1 \right)^{1-\lambda_c} \quad (9)$$

where P_c is capillary pressure, P_a is atmospheric pressure, S_{rw} is residual saturation of water, and λ_c is the empirical-fit coefficient.

Relative permeability models are set based on improved Corey–Stone equation.

$$K_{rw} = \left(\frac{S_w - S_{rw}}{1 - S_{rw}} \right)^{n_w} \quad (10)$$

$$K_{rg} = \left(\frac{S_g - S_{rg}}{1 - S_{rg}} \right)^{n_g} \quad (11)$$

where K_{rw} is relative permeability of water phase, K_{rg} is relative permeability of gas phase, and n_w and n_g are empirical-fit coefficients.

2.2. Mathematical Model for Decomposition of Natural-Gas Hydrate

The decomposition of natural-gas hydrate is a complex process combining heat and mass transfer with phase change, and is mainly controlled by two-phase seepage flow of gas and liquid, the heat-transfer process, and kinetics of hydrate decomposition. The mathematical model of natural-gas-hydrate decomposition is established based on the equation of conservation of mass, the equation of conservation of energy, and the equation of kinetics for hydrate decomposition.

2.2.1. Conservation of Mass

Considering only the presence of gas, liquid, and solid phases, where the gas phase is methane, the liquid phase is water, and the solid phase is natural-gas hydrate, the natural-gas hydrate fills the porous medium, the gas and liquid phases flow through the porous medium, and the fluid flow obeys Darcy's law.

$$R_g = \frac{\partial(\varphi\rho_g S_g)}{\partial t} + \frac{1}{r} \frac{\partial(r\rho_g v_{gr})}{\partial r} + \frac{\partial(\rho_g v_{gz})}{\partial z} \quad (12)$$

where R_g is rate of gas production, ρ_g is density of gas, and S_g is saturation of gas.

$$v_{gr} = -\frac{Kk_{rg}}{\mu_g} \frac{\partial P_g}{\partial r} \quad (13)$$

$$v_{gz} = -\frac{Kk_{rg}}{\mu_g} \frac{\partial(P_g - G_g)}{\partial z} \quad (14)$$

where v_{gr} is seepage-flow velocity of gas in the r-direction, K is absolute permeability of porous media, k_{rg} is relative permeability of gas, μ_g is viscosity of gas, P_g is pressure of the gas phase, v_{gz} is seepage-flow velocity of gas in the z-direction, and G_g is gravity of gas.

$$R_w = \frac{\partial(\varphi\rho_w S_w)}{\partial t} + \frac{1}{r} \frac{\partial(r\rho_w v_{wr})}{\partial r} + \frac{\partial(\rho_w v_{wz})}{\partial z} \quad (15)$$

where R_w is rate of water production, ρ_w is density of water, and S_w is saturation of water.

$$v_{wr} = -\frac{Kk_{rw}}{\mu_w} \frac{\partial P_w}{\partial r} \quad (16)$$

$$v_{wz} = -\frac{Kk_{rw}}{\mu_w} \frac{\partial(P_w - G_w)}{\partial z} \quad (17)$$

where v_{wr} is seepage-flow velocity of water in the r-direction, k_{rw} is relative permeability of water, μ_w is viscosity of water, P_w is pressure of water, v_{wz} is seepage-flow velocity of water in the z-direction, and G_w is gravity of water.

2.2.2. Conservation of Energy

The conservation of energy of the whole reservoir can be expressed by the temperature and the enthalpy change of each component considering heat injection, heat conduction, heat convection, and heat absorption by hydrate decomposition.

$$Q_{hd} + Q_{in} = \frac{\partial}{\partial t} [(1 - \varphi)\rho_p h_p + \varphi S_h \rho_h h_h + \varphi S_g \rho_g h_g + \varphi S_w \rho_w h_w] \\ + \frac{1}{r} \frac{\partial}{\partial r} (x\rho_g v_{gr} h_g + r\rho_w v_{wr} h_w) + \frac{\partial}{\partial z} (\rho_g v_{gz} h_g + \rho_w v_{wz} h_w) \\ + \frac{1}{r} \frac{\partial}{\partial r} (r\lambda_r \frac{\partial T}{\partial r}) + \frac{\partial}{\partial z} (\lambda_r \frac{\partial T}{\partial z}) \quad (18)$$

where Q_{hd} is heat absorbed by the decomposition of hydrates, Q_{in} is heat by injection, λ_r is thermal conductivity of the entire reservoir, φ_f is porosity occupancy of fluid, and φ_p is porosity occupancy of porous media.

$$\lambda_r = \varphi_f(\lambda_w S_w + \lambda_g S_g) + (1 - \varphi_p)\lambda_p + (\varphi_p - \varphi_f)\lambda_h \quad (19)$$

where λ_w is thermal conductivity of water, λ_g is thermal conductivity of gas, and λ_h is thermal conductivity of hydrate.

$$Q_{hd} = R_h q_{hd} = R_p h_p + R_g h_g + R_w h_w \quad (20)$$

where R_h is rate of hydrate decomposition and q_{hd} is heat absorbed rate by the decomposition of hydrates.

$$dh_h = C_h dT \quad (21)$$

$$dh_g = C_g dT + \sigma_g P_g \quad (22)$$

$$\sigma_g = \left(\frac{\partial h_g}{\partial p_g} \right)_T \quad (23)$$

$$dh_w = C_w dT \quad (24)$$

$$dh_p = C_p dT \quad (25)$$

where C_h is isobaric specific heat capacity of hydrates, C_g is isobaric specific heat capacity of gas, σ_g is throttling coefficient of gas, C_w is isobaric specific heat capacity of water, and C_p is isobaric specific heat capacity of porous media.

2.2.3. Kinetics for Hydrate Decomposition

The equation of kinetics for the decomposition of natural-gas hydrate is as below:

$$R_h = \frac{\partial(\varphi \rho_h S_h)}{\partial t} \quad (26)$$

where R_h is rate of hydrate decomposition, ρ_h is density of the hydrate, S_h is saturation of the hydrate, φ is porosity, and t is time.

Considering only SI natural-gas hydrate, the molecular formula of natural-gas hydrate is assumed to be $8\text{CH}_4 \cdot 46\text{H}_2\text{O}$.

$$R_h = -R_g \frac{M_h}{M_g} \quad (27)$$

$$R_g = M_g k_d A_s (f_e - f_g) = M_g k_d A_s (P_e - P_g) \quad (28)$$

$$R_w = 5.75 m_g \frac{M_w}{M_g} \quad (29)$$

where R_h is rate of hydrate decomposition, ρ_h is density of the hydrate, M_h is molar mass of hydrate, M_g is molar mass of gas, M_w is molar mass of water, A_s is total surface area of hydrate, k_d is reaction kinetic coefficient for hydrate, f_e is fugacity of three-phase equilibrium, f_g is fugacity of gas, P_e is pressure of three-phase equilibrium, and P_g is pressure of gas.

$$k_d = k_d^i e^{-\frac{\Delta E_a}{RT_e}} \quad (30)$$

$$A_s = \varphi_i (1 - S_h) \cdot \sqrt{\frac{\varphi_i (1 - S_h)}{2K_i}} \quad (31)$$

$$P_e = 1.15 e^{(49.3185 - \frac{9459}{T_e})} \quad (32)$$

where k_d is reaction kinetic coefficient for hydrates, k_{di} is intrinsic decomposition coefficient for hydrates, E_a is apparent activation energy for decomposition, T_e is equilibrium temperature, A_s is total surface area of hydrates, P_e is pressure of three-phase equilibrium, K_i is initial permeability of the reservoir, φ_i is initial porosity, and S_h is saturation of hydrate.

$$R_g = M_g k_d^i e^{-\frac{\Delta E_a}{RT_e}} \varphi_i (1 - S_h) \cdot \sqrt{\frac{\varphi_i (1 - S_h)}{2K_i}} (P_e - P_g) \quad (33)$$

2.3. Setting for Model of Natural-Gas-Hydrate Reservoir

A two-dimensional radially symmetric reservoir containing natural-gas hydrate is considered (Figure 1). The upper and lower cover layers, defined as the overburden and underburden of the reservoir are non-permeable cover layers, and there is heat exchange between the reservoir and cover layers. A straight well is set in the center of the model for heat injection and gas production, and a perforation point is set close to the bottom of the well.

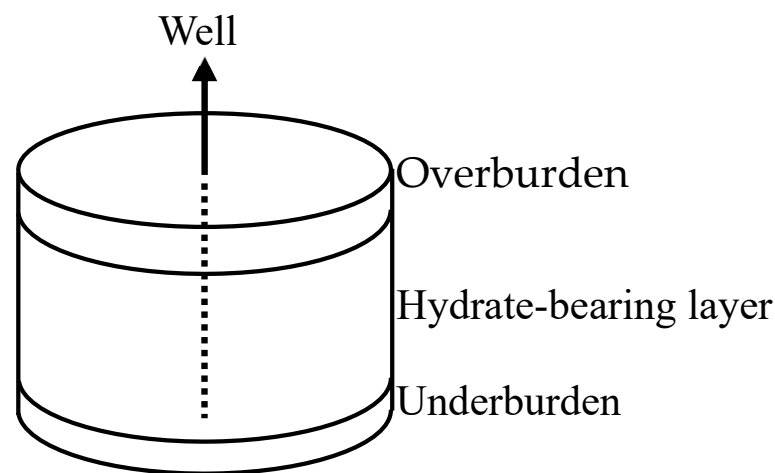


Figure 1. Schema of two-dimensional radially symmetric reservoir containing natural-gas hydrate with overburden and underburden.

2.3.1. Basic Parameters

Basic parameters of the natural-gas-hydrate reservoir model were set according to a typical natural-gas-hydrate reservoir [13,37]. Density of water was set to 1000 kg/m^3 , density of hydrate was 900 kg/m^3 , density of rock was 2500 kg/m^3 , and density of methane was 0.75 kg/m^3 . Thermal conductivity of water was $0.59 \text{ W/(m}\cdot\text{K)}$, thermal conductivity of hydrate was $0.53 \text{ W/(m}\cdot\text{K)}$, thermal conductivity of rock was $10.00 \text{ W/(m}\cdot\text{K)}$, and thermal conductivity of methane was $0.03 \text{ W/(m}\cdot\text{K)}$. Specific heat capacity of hydrate was $3.00 \text{ KJ/(kg}\cdot\text{K)}$, specific heat capacity of methane was $2.07 \text{ KJ/(kg}\cdot\text{K)}$, specific heat capacity of water was $4.20 \text{ KJ/(kg}\cdot\text{K)}$, and specific heat capacity of rock was $0.76 \text{ KJ/(kg}\cdot\text{K)}$.

Kinetic parameters of natural-gas-hydrate decomposition were determined using transparent-kettle experimental apparatus [37]. Molecular mass was 0.119 kg/mol , molar density was $0.919 \times 10^3 \text{ kg/mol}$, molar volume was $7.696 \times 10^3 \text{ m}^3/\text{mol}$, response frequency was 1.071×10^{13} , activation energy was 8.108×10^4 , and reaction enthalpy was 5.186×10^4 .

2.3.2. Gridding

Small grid size was used in the model to describe the temperature and saturation distribution of the hydrate reservoir in detail. A cylindrical model with radius of 5 m and height of 7 m was created. The model had 100 grids, divided radially with grid size of 0.05 m; 120 grids divided longitudinally with 10 grids at the top as the overburden; and 10 grids at the bottom as the underburden. A straight well was set in the center of the model for heat injection and gas production, the perforation point for heat injection was set at 1 m, 20 grids away from underburden, and the perforation point for gas production is set at 1 m, 20 grids away from overburden (Figure 2).

2.3.3. Initial Conditions

Considering the condition that hydrates can be uniformly distributed in porous media, the porosity of the entire hydrate reservoir was set to 0.35, and the pressure of the entire hydrate reservoir was set to 5 MPa. Permeability of the hydrate-bearing reservoir was set to $500 \times 10^{-3} \mu\text{m}^2$, and permeability of overburden and underburden were set to 0. Saturation of water in the hydrate-bearing layer was set to 0.5, and saturation of water in the overburden and underburden was set to 1.0. Saturation of hydrate in the hydrate-bearing layer was set to 0.5, and saturation of hydrate in overburden and underburden was set to 0. The temperature of hydrate in hydrate-bearing layer was set to $1.0 \text{ }^\circ\text{C}$.

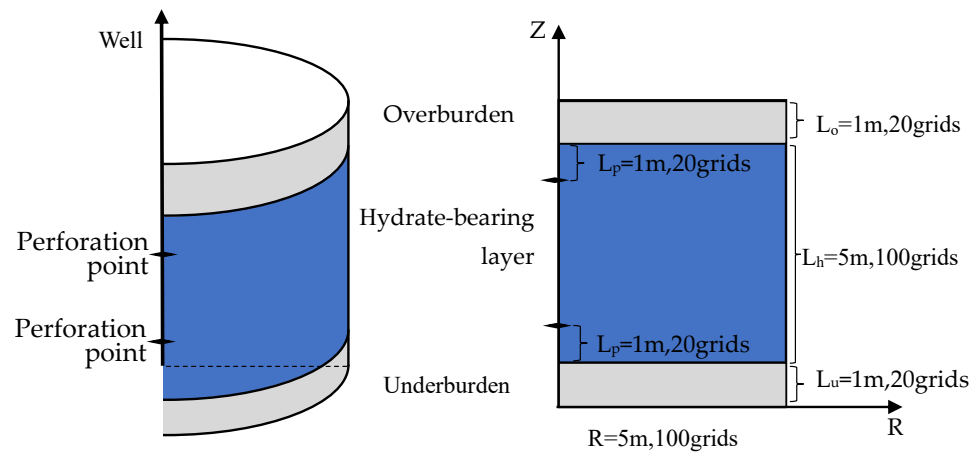


Figure 2. Grid setting of model.

2.3.4. Boundary Conditions

There was no heat or mass transfer between the natural-gas-hydrate reservoir model and the outside, as there was no heat and mass flow through the boundary of the model.

$$T|_{r=0, Z=0} = T_i \quad (34)$$

$$\frac{\partial T}{\partial t}|_{r=0, Z=L} = 0 \quad (35)$$

$$S_h|_{r=0, Z=0} = S_{hi} \quad (36)$$

$$\frac{\partial S_h}{\partial t}|_{r=0, Z=L} = 0 \quad (37)$$

where T_i is initial formation temperature, L is the height of the model, and S_{hi} is the initial saturation of hydrate.

$$P|_{r=0, Z=0} = P_i \quad (38)$$

$$\frac{\partial P}{\partial t}|_{r=0, Z=L} = 0 \quad (39)$$

$$\frac{\partial P}{\partial r}|_{r=0} = 0 \quad (40)$$

$$\frac{\partial P}{\partial r}|_{r=R} = 0 \quad (41)$$

$$\frac{\partial P}{\partial z}|_{z=L} = 0 \quad (42)$$

where P_i is initial formation pressure and R is radius of the model.

3. Results and Discussion

Based on the modeling section above, numerical simulations of natural-gas-hydrate decomposition in the process of heat-injection production were carried out to quantitatively calculate the daily and cumulative gas production, and to qualitatively analyze the characteristics of temperature distribution, saturation distribution, and decomposition-front movement in the reservoir. The effects of temperature and rate of heat injection on temperature distribution, saturation distribution, and decomposition-front movement in a natural-gas-hydrate reservoir were simulated and are discussed, and the decomposition process and heat- and mass-transfer law of natural-gas hydrate in the process of heat-injection production are clarified.

3.1. Production

The process of “lower heat injection, upper natural gas extraction” was adopted, where the injection well and production well are located in the center of the reservoir. The injection well was perforated at 1 m, 20 grids away from underburden in the axial direction (Figure 2), and the production well was perforated at 1 m, 20 grids away from overburden. Hot water of a certain heat-injection temperature was continuously injected at a certain heat-injection rate for a period of time. Heat-injection temperature was set to 50 °C, 70 °C, and 90 °C while heat-injection rate was fixed to be 50 m³/day. Heat-injection rate was set to 10 m³/day, 30 m³/day, and 50 m³/day while heat-injection temperature was fixed to be 90 °C. Cumulative production and daily production for 150 days at different heat-injection temperatures and heat-injection rates were calculated and further analyzed based on results of numerical simulations.

3.1.1. Cumulative Production

The final cumulative production was approximately equivalent for different heat-injection temperatures with a constant heat-injection rate of 50 m³/day, as there was sufficient injection heat to ensure complete decomposition of hydrates. Cumulative production reached a maximum of about 9600 m³ as the final cumulative production for different heat-injection temperatures (Figure 3).

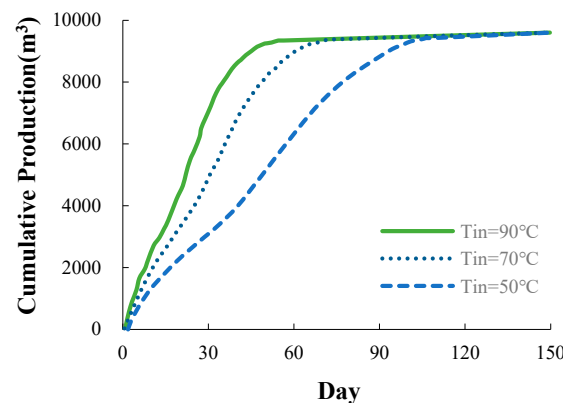


Figure 3. Cumulative production for different heat-injection temperatures.

Cumulative production reached a maximum after 63 days when the heat-injection temperature was 90 °C; this was the fastest of the three different injection temperatures. Cumulative production reached a maximum after 78 days when the heat-injection temperature was 70 °C, and cumulative production reached a maximum after 117 days when the heat-injection temperature was 50 °C.

The final cumulative production was approximately equivalent for the different heat-injection rates with a constant heat-injection temperature of 90 °C, as this was sufficient injection heat to ensure complete decomposition of hydrates. Cumulative production reached a maximum of about 9600 m³ for the different heat-injection rates (Figure 4).

Cumulative production reached a maximum after 63 days when the heat-injection rate was 50 m³/day; this was the fastest of the three different injection temperatures. Cumulative production reached a maximum after 95 days when the heat-injection rate was 30 m³/day and after 135 days when the heat-injection rate was 10 m³/day.

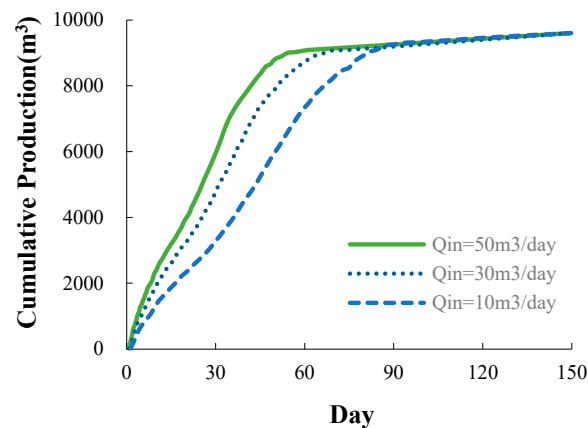


Figure 4. Cumulative production for different heat-injection rates.

3.1.2. Daily Production

On the whole, daily production for different heat-injection temperatures with a constant heat-injection rate of $50 \text{ m}^3/\text{day}$ showed similar variation patterns (Figure 5), with daily production rising rapidly to a peak at the beginning, gradually decreasing to a certain value, then showing a certain magnitude of increase, and then decreasing slowly until the final daily gas production was $0 \text{ m}^3/\text{day}$.

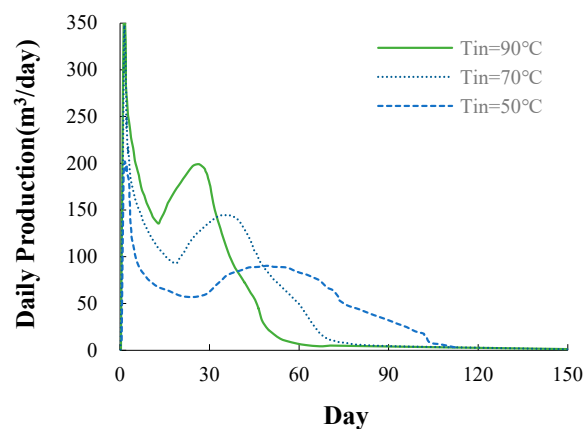


Figure 5. Daily production for different heat-injection temperatures.

The effective gas permeability was greater in the initial stage of heat-injection production, and daily production increased rapidly. The trend in daily gas production was relatively flat when the heat-injection temperature was $50 \text{ }^\circ\text{C}$ and there were large fluctuations in daily gas production when the heat-injection temperature was $90 \text{ }^\circ\text{C}$. Therefore, variation in daily gas production increased with increase in heat-injection temperature. When the heat-injection temperature was $50 \text{ }^\circ\text{C}$, $70 \text{ }^\circ\text{C}$, and $90 \text{ }^\circ\text{C}$, daily gas production trended to $0 \text{ m}^3/\text{day}$ at 115 days, 78 days, and 62 days, respectively, indicating that the higher heat-injection temperature was more favorable for the rapid decomposition of hydrates.

Daily production for different heat-injection rates with a constant heat-injection temperature of $90 \text{ }^\circ\text{C}$ showed similar variation patterns on the whole (Figure 6), with daily production rising rapidly to a peak at the beginning, gradually decreasing to a certain value, then showing a certain magnitude of increase, and then decreasing slowly until the final daily gas production was $0 \text{ m}^3/\text{day}$.

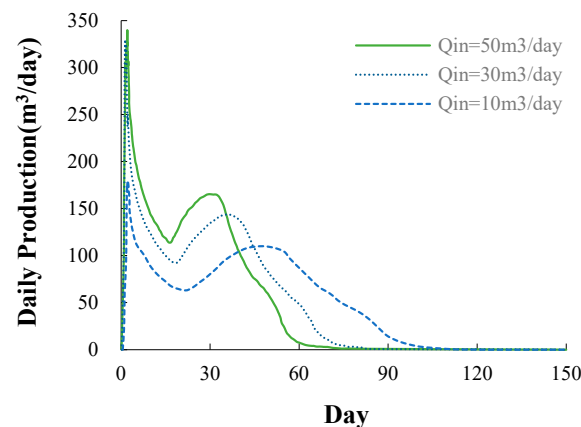


Figure 6. Daily production for different heat-injection rates.

In the initial stage of heat-injection production, a large amount of hydrate decomposed rapidly to produce a large amount of natural gas, and daily production increased rapidly. Daily gas production decreased gradually during the time of heat transfer to the hydrate-decomposition zone. With the continuous heat injection, a large amount of hydrate in the hydrate decomposition zone began to decompose, and gas production rate decreased and then increased.

3.2. Decomposition Characteristics

Characteristics of the temperature distribution, saturation distribution, and decomposition front in the reservoir for different heat-injection temperatures and heat-injection rates can be analyzed and further discussed based on results of numerical simulation, taking 2 days, 10 days, and 50 days in the process of heat-injection production as comparison points for decomposition characteristics of different heat-injection temperatures and heat-injection rates. Heat-injection temperature was set to 50 °C, 70 °C, and 90 °C while heat-injection rate was fixed to be 50 m³/day, and heat-injection rate was set to 10 m³/day, 30 m³/day, and 50 m³/day while heat-injection temperature was fixed to be 90 °C.

3.2.1. Temperature Distribution

The overall temperature distribution contours were similar for different heat-injection temperatures or different heat-injection rates, and the temperature-distribution contours' sparsity could be seen as "sparse-dense-sparse" as the distance to the injection well increased. Natural-gas hydrate in the vicinity of the wells was completely decomposed, while the continuous injection of heat prevented steep changes in temperature, which was reflected in a relatively sparse temperature-contour distribution. The intermediate area had a relatively pronounced change in temperature over a smaller area due to the large amount of heat absorbed by the decomposition of natural-gas hydrate leading to a sharp drop in temperature, and resulting in a denser contour. In the area far from the injection well, heat could only be transferred forward by thermal conductivity. The process of thermal-conductivity transfer was slow and no large changes in temperature occurred within a small area, which is reflected in the relatively sparse contours.

Temperature-distribution contours for different heat-injection temperatures with a constant heat-injection rate of 50 m³/day showed that the overall trend of temperature decreasing along the injection-production direction with heat injection remaining similar, despite the heat-injection temperature varying from 50 °C to 70 °C and 90 °C (Figure 7). Temperature was higher around the injection well and lower away from the injection well, with faster temperature propagation along the injection-production direction with heat injection, which indicates that convective heat transfer is the main mode of heat propagation in process of heat-injection production of natural-gas hydrate. The maximum temperature contour moved faster at a heat-injection temperature of 90 °C compared to 70 °C or 50 °C,

as the temperature difference between injection fluid and the hydrate reservoir increased, and more heat was transferred forward in the same time.

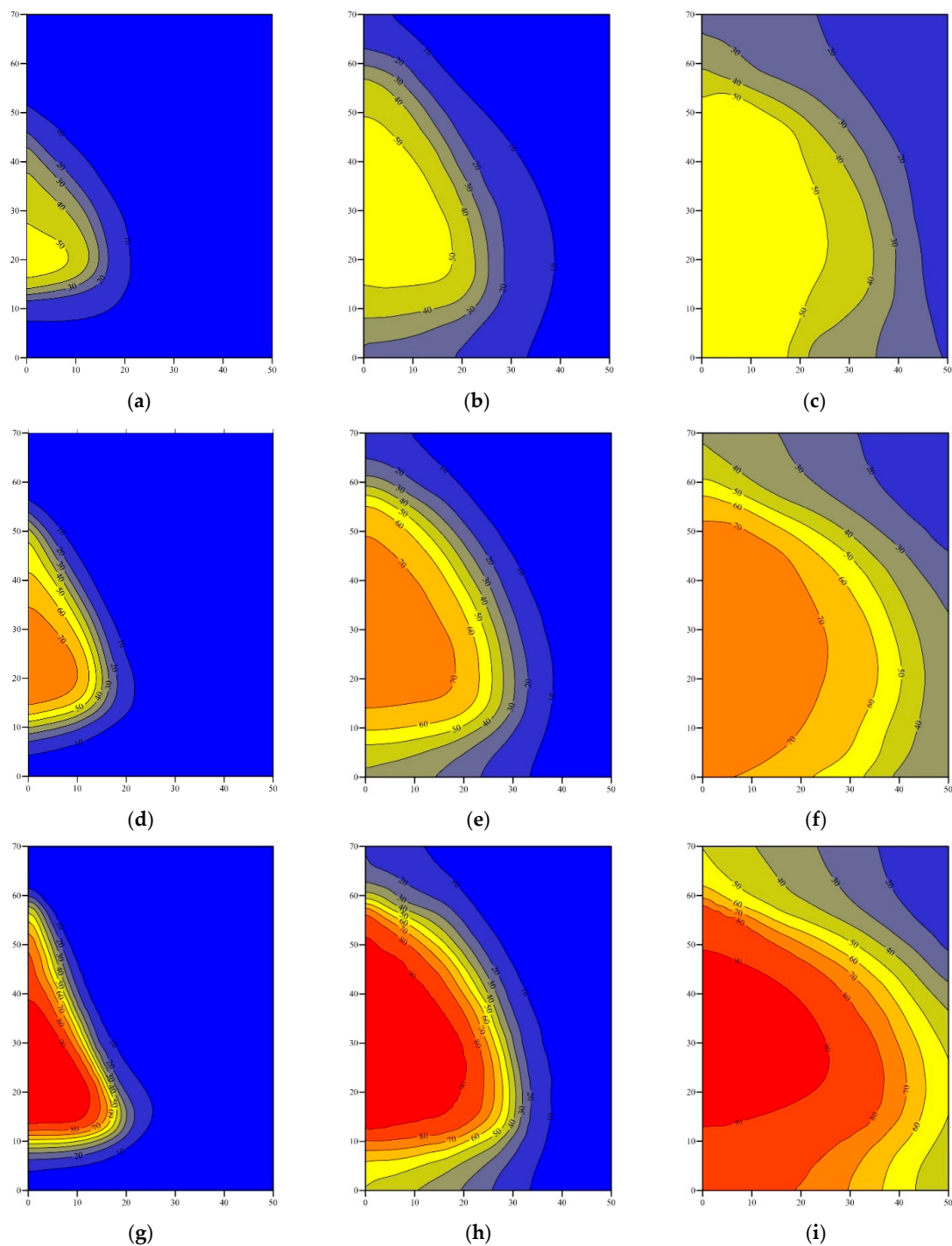


Figure 7. Temperature distribution for different heat-injection temperatures. (a) $T_{in} = 50\text{ }^{\circ}\text{C}$ after 2 days; (b) $T_{in} = 50\text{ }^{\circ}\text{C}$ after 10 days; (c) $T_{in} = 50\text{ }^{\circ}\text{C}$ after 50 days; (d) $T_{in} = 70\text{ }^{\circ}\text{C}$ after 2 days; (e) $T_{in} = 70\text{ }^{\circ}\text{C}$ after 10 days; (f) $T_{in} = 70\text{ }^{\circ}\text{C}$ after 50 days; (g) $T_{in} = 90\text{ }^{\circ}\text{C}$ after 2 days; (h) $T_{in} = 90\text{ }^{\circ}\text{C}$ after 10 days; (i) $T_{in} = 90\text{ }^{\circ}\text{C}$ after 50 days.

Temperature-distribution contours for different heat-injection rates with a constant heat-injection temperature of $90\text{ }^{\circ}\text{C}$ showed that the temperature was close to $90\text{ }^{\circ}\text{C}$ around the injection well, and temperature decreased along the injection-production direction with heat injection and with faster temperature propagation (Figure 8), as convective heat

transfer is the main mode of heat propagation in process of heat-injection production of natural-gas hydrate. Temperature-distribution contours were dense in the middle section and sparse on the sides, indicating rapid temperature change in the middle section. The overall temperature after the same simulation time was higher for higher injection rates, and the highest temperature contour was further away from the injection well. The high-temperature area was larger as the heat-injection rate increased, indicating that the heat-injection rate had a greater effect on the decomposition of natural-gas hydrate within the reservoir.

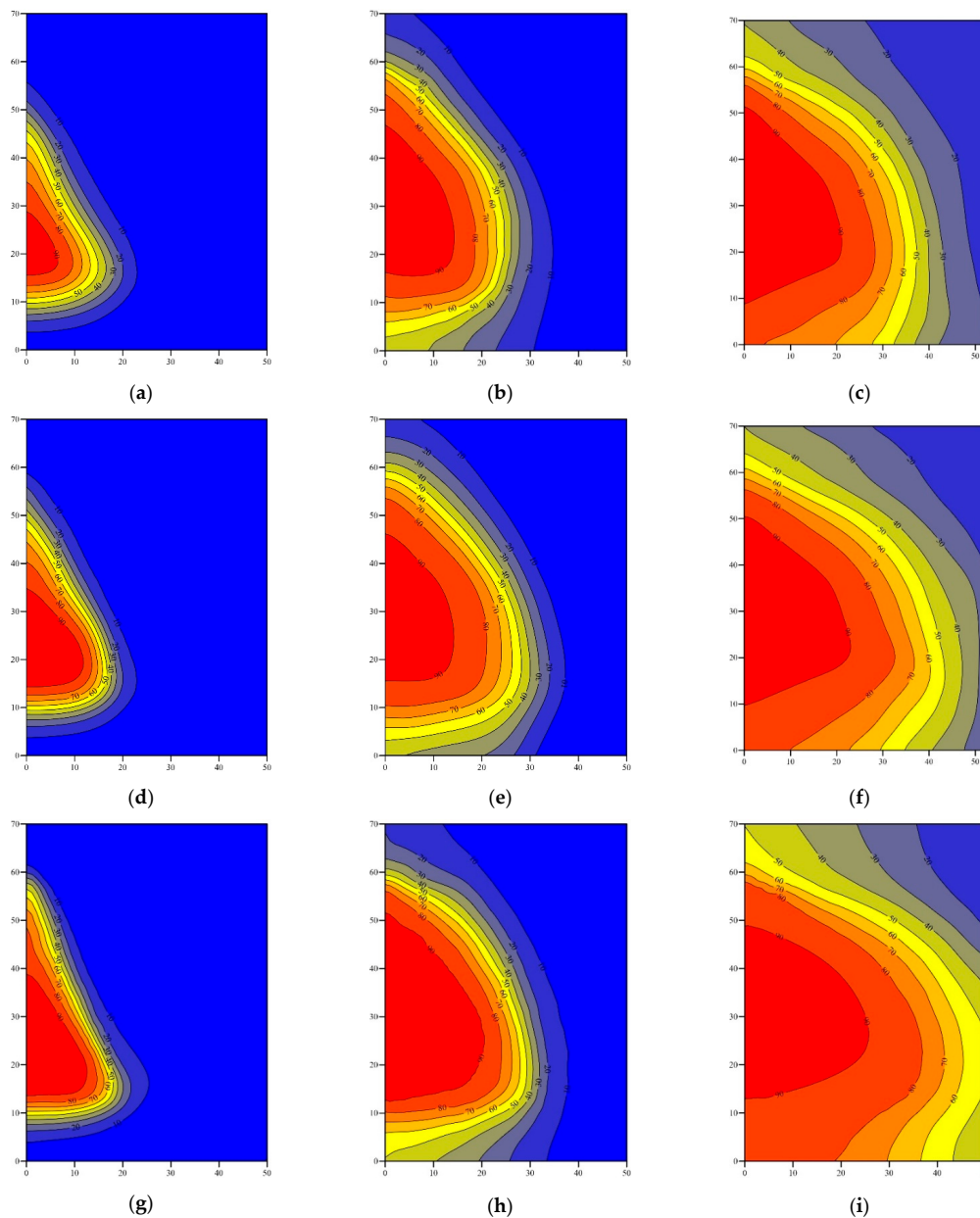


Figure 8. Temperature distribution for different heat-injection rates. (a) $Q_{in} = 10 \text{ m}^3/\text{day}$ after 2 days; (b) $Q_{in} = 10 \text{ m}^3/\text{day}$ after 10 days; (c) $Q_{in} = 10 \text{ m}^3/\text{day}$ after 50 days; (d) $Q_{in} = 30 \text{ m}^3/\text{day}$ after 2 days; (e) $Q_{in} = 30 \text{ m}^3/\text{day}$ after 10 days; (f) $Q_{in} = 30 \text{ m}^3/\text{day}$ after 50 days; (g) $Q_{in} = 50 \text{ m}^3/\text{day}$ after 2 days; (h) $Q_{in} = 50 \text{ m}^3/\text{day}$ after 10 days; (i) $Q_{in} = 50 \text{ m}^3/\text{day}$ after 50 days.

3.2.2. Saturation Distribution

The overall saturation distribution contours of natural gas hydrates show a similar pattern, showing an outward convex trend along the injection-production direction with

heat injection (Figure 9). The outward convex saturation-distribution contour around the injection-well bore was more backward, which indicates that the natural-gas hydrate decomposed faster around the injection-well bore. The outward convex saturation-distribution contour gradually moved forward as simulation time progressed with heat injection.

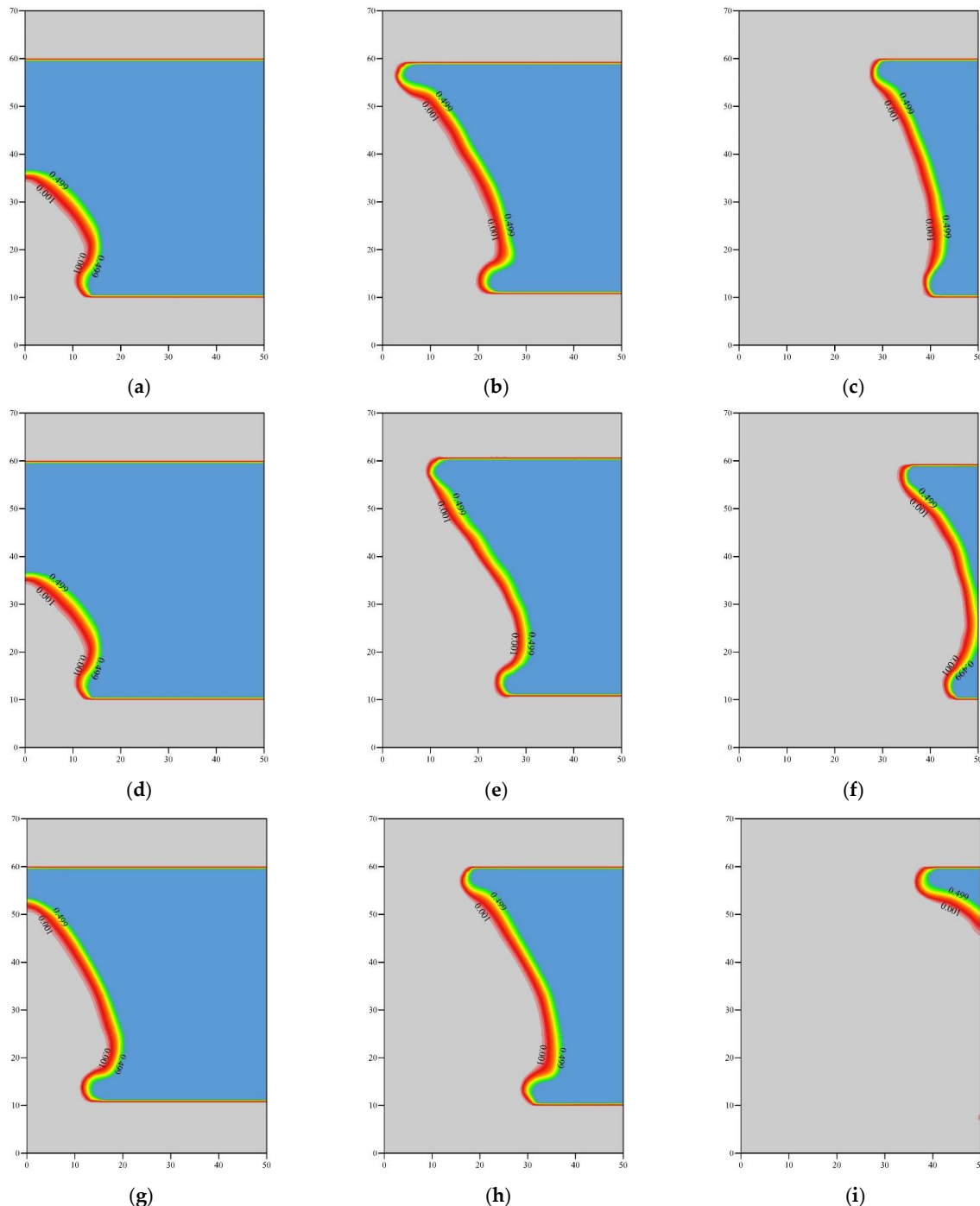


Figure 9. Saturation distribution for different heat-injection temperatures. (a) $T_{in} = 50\text{ }^{\circ}\text{C}$ after 2 days; (b) $T_{in} = 50\text{ }^{\circ}\text{C}$ after 10 days; (c) $T_{in} = 50\text{ }^{\circ}\text{C}$ after 50 days; (d) $T_{in} = 70\text{ }^{\circ}\text{C}$ after 2 days; (e) $T_{in} = 70\text{ }^{\circ}\text{C}$ after 10 days; (f) $T_{in} = 70\text{ }^{\circ}\text{C}$ after 50 days; (g) $T_{in} = 90\text{ }^{\circ}\text{C}$ after 2 days; (h) $T_{in} = 90\text{ }^{\circ}\text{C}$ after 10 days; (i) $T_{in} = 90\text{ }^{\circ}\text{C}$ after 50 days.

The saturation of natural-gas hydrate along with the boundary of the reservoir changed from 0.5 to 0 within one grid (Figure 9), as overburden and underburden of the reservoir are non-permeable cover layers and there was no heat and mass flow through the boundary of

the reservoir. The saturation-distribution contours for different heat-injection temperatures or different heat-injection rates show uniformly prominent features, i.e., saturation of natural-gas hydrate steeply changed from 0.5 to 0 in a narrow area, indicating that natural-gas-hydrate decomposition occurred only in this area. The saturation distribution can be clearly divided into three areas: constant 0.5 saturation area, saturation steeply changing area, and constant 0 saturation area, so the reservoir can be divided into three different areas: hydrate area, gas/water/hydrate area, and gas/water area.

Saturation-distribution contours for different heat-injection temperatures with a constant heat-injection rate of $50 \text{ m}^3/\text{day}$ showed that the outward convex trend along the injection-production direction with heat injection remained similar, despite the heat-injection temperature varying from $50 \text{ }^\circ\text{C}$ to $70 \text{ }^\circ\text{C}$ and $90 \text{ }^\circ\text{C}$ (Figure 9). The outward convex trend was more obvious as heat-injection temperature increased. Saturation of natural-gas hydrate was 0 around the injection well and was close to 0.5 away from the injection well, which indicates that natural-gas hydrate fully decomposes in the process of heat-injection production of natural-gas hydrate. The decomposition zone was clearly narrow at the top and wide at the bottom, indicating that decomposition of natural-gas hydrate was faster below the reservoir and slower above. The non-decomposition zone gradually decreased as the simulation time advanced, and the non-decomposition zone was smaller when the heat-injection temperature was higher.

Saturation-distribution contours for different heat-injection rates with a constant heat-injection temperature of $90 \text{ }^\circ\text{C}$ showed that the outward convex trend along the injection-production direction with heat injection remained similar, despite the heat-injection temperature varying from $10 \text{ m}^3/\text{day}$ to $30 \text{ m}^3/\text{day}$ and $50 \text{ m}^3/\text{day}$ (Figure 10). The outward convex trend was more obvious as heat-injection rate increased. The decomposition zone increased as the simulation time advanced, and the decomposition zone was larger when the heat-injection rate was higher.

3.2.3. Decomposition Front

The decomposition of natural-gas hydrate is not of the piston type. There was narrow area where decomposition occurred and saturation of natural-gas hydrate changed steeply from 0.5 to 0 in a narrow area. The area where there is a rapid increase in saturation distribution, and where the natural-gas hydrate is decomposing, is defined as decomposition front. The decomposition front occurs due to the rapid increase in temperature of the heat injection. This is an instantaneous contact process that takes place during heat injection, and the decomposition gas and water flow rapidly away from the decomposition front under certain pressure differences. Comparing coordinates of the decomposition front with coordinates of the temperature distribution, it can be seen that the contours with temperatures of $15\text{--}17 \text{ }^\circ\text{C}$ coincided with the decomposition front, which indicates that the temperature at the decomposition front was about $15\text{--}17 \text{ }^\circ\text{C}$.

With the increase in the heat-injection rate at constant heat-injection temperature, the decomposition front moves faster, but the amplitude decreases (Figure 9), which is due to the fact that the higher the heat-injection rate, the more heat is obtained by the reservoir, and the faster the decomposition front moves. With the increase in heat-injection temperature at constant heat-injection rate, the decomposition front moved faster while the heat loss to the surrounding strata increased as the heat injection rate decreased, therefore, the decomposition front moved faster but the amplitude decreased (Figure 10). The reason for this is that the higher the heat-injection temperature, the greater the heat loss and the less heat available for hydrate decomposition.

From the perspective of saturation distribution of natural-gas hydrate, the reservoir can be divided into three different areas: hydrate area (saturation of natural-gas hydrate is close to the initial value of 0.5), gas/water/hydrate area (saturation of natural-gas hydrate is between 0 and 0.5), and gas/water area (saturation of natural-gas hydrate is 0). From the perspective of the decomposition front, the reservoir can be divided into three different areas: the non-decomposition zone, the decomposing zone, and the decomposition zone.

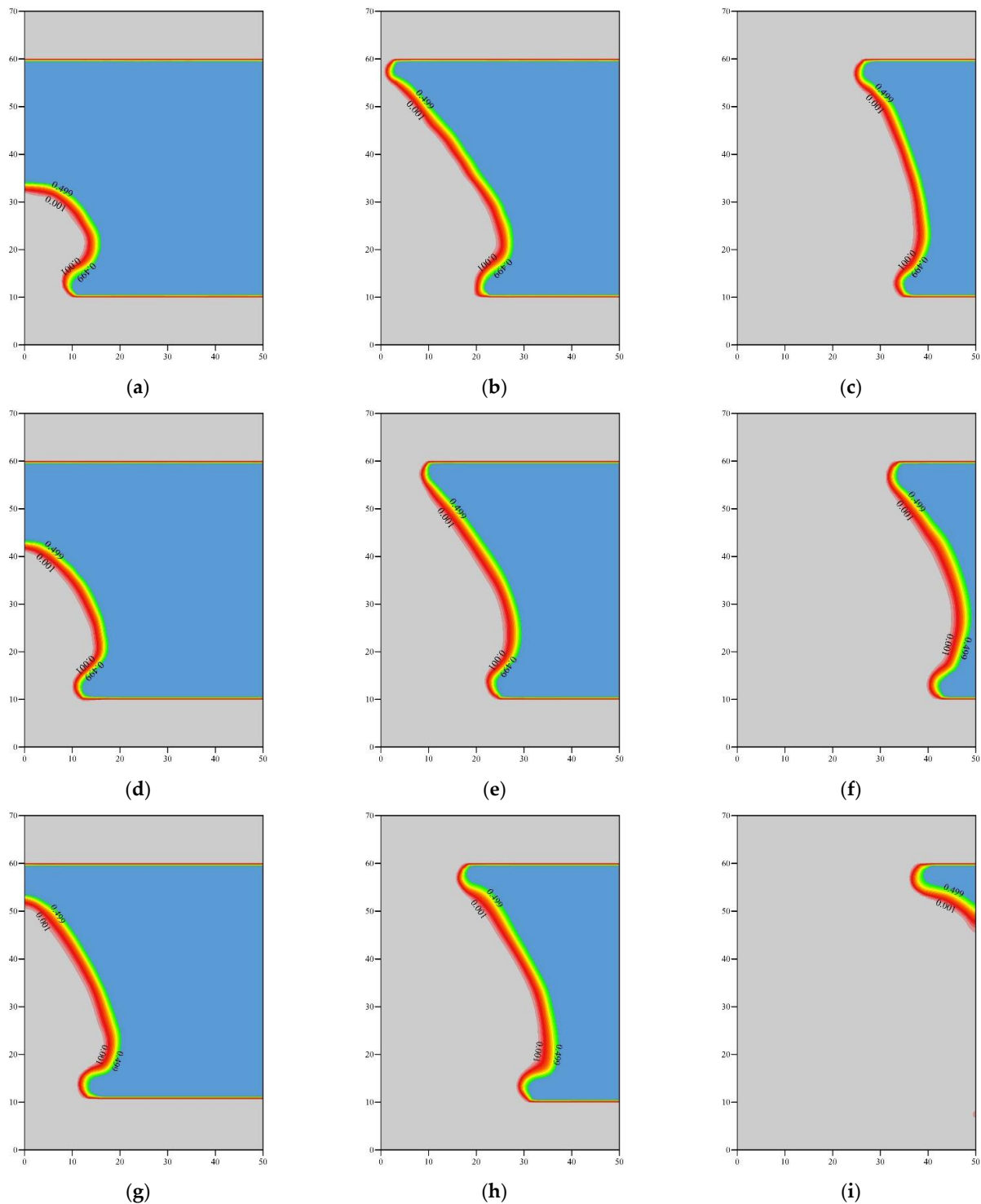


Figure 10. Saturation distribution for different heat-injection rates. (a) $Q_{in} = 10 \text{ m}^3/\text{day}$ after 2 days; (b) $Q_{in} = 10 \text{ m}^3/\text{day}$ after 10 days; (c) $Q_{in} = 10 \text{ m}^3/\text{day}$ after 50 days; (d) $Q_{in} = 30 \text{ m}^3/\text{day}$ after 2 days; (e) $Q_{in} = 30 \text{ m}^3/\text{day}$ after 10 days; (f) $Q_{in} = 30 \text{ m}^3/\text{day}$ after 50 days; (g) $Q_{in} = 50 \text{ m}^3/\text{day}$ after 2 days; (h) $Q_{in} = 50 \text{ m}^3/\text{day}$ after 10 days; (i) $Q_{in} = 50 \text{ m}^3/\text{day}$ after 50 days.

Area share is proposed to characterize the decomposition characteristics of natural-gas hydrate. The total of the area share of the non-decomposition zone, the decomposing zone, and the decomposition zone is 100%. Area share of the decomposing zone, i.e., the dissociation front, is fixed at 1% due to the small area share and large morphological

variation. Area share of the decomposing zone changes because of decomposition of natural-gas hydrate in the process of heat-injection production.

Area share of the decomposition zone of different heat-injection rates and heat-injection temperatures at the same comparison point (Figure 11) shows that area share of decomposition zone was highest when the heat-injection rate was 50 m³/day and the heat-injection temperature was 90 °C, which means that decomposition of hydrate was better with a higher heat-injection rate and higher heat-injection temperature. Meanwhile, area share of decomposition zone was lowest with the highest heat-injection temperature of 90 °C, while heat-injection rate was lowest at 10 m³/day, which indicates that, to some extent, heat-injection rate has more influence on decomposition of hydrate than heat-injection temperature.

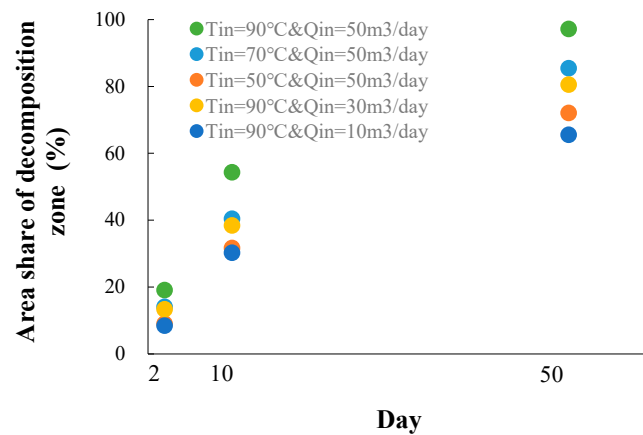


Figure 11. Area share of decomposition zone at different comparison points.

Area share of the decomposition zone for different heat-injection temperatures with a constant heat-injection rate of 50 m³/day at the same comparison point (Table 1) shows that area share of decomposition zone after 2 days of heat injection was 9.025%, 14.042%, and 19.085% with heat-injection temperatures of 50 °C, 70 °C, and 90 °C, respectively, and the increase extent was 155.587% and 135.908%. Area share of the decomposition zone at other comparison points also showed a similar pattern of variation, i.e., area share of decomposition zone increased as heat-injection temperature increased, but the rate of increase reduced. High heat-injection temperature does not play a more significant role than heat-injection rate in promoting the decomposition of natural-gas hydrate. When the heat-injection temperature was higher than 90 °C, the area share of decomposition zone did not increase significantly. The reason for this is that the higher the heat-injection temperature, the greater the heat loss, meaning that less heat will be available for hydrate decomposition.

Table 1. Area share of decomposition zone for different heat-injection temperatures.

Comparison Point	Heat-Injection Rate	Area Share (%)			
		Decomposing Zone	Non-Decomposition Zone	Decomposition Zone	Increase Extent
After 2 days	Q _{in} = 10 m ³ /day		90.592	8.408	/
	Q _{in} = 30 m ³ /day		86.695	12.305	146.341
	Q _{in} = 50 m ³ /day		79.915	19.085	155.096
After 10 days	Q _{in} = 10 m ³ /day	1	68.763	30.237	/
	Q _{in} = 30 m ³ /day		58.902	40.098	132.612
	Q _{in} = 50 m ³ /day		44.703	54.297	135.409
After 50 days	Q _{in} = 10 m ³ /day		33.458	65.542	/
	Q _{in} = 30 m ³ /day		19.341	79.659	121.539
	Q _{in} = 50 m ³ /day		1.797	97.203	122.024

Area share of the decomposition zone for different heat-injection rates with a constant heat-injection temperature of 90 °C at the same comparison point (Table 2) shows that the area share of the decomposition zone increased as the heat-injection rate increased. Area share of the decomposition zone after 2 days of heat injection was 8.408%, 12.305%, and

19.085% when the heat-injection rate was 10 m³/day, 30 m³/day, and 50 m³/day, respectively, and the increase extent was 146.341% and 155.096%. Area share of the decomposition zone at other comparison points showed a similar pattern of variation, i.e., area share of decomposition zone increased as heat-injection rate increased, and the increase extent also increased. The high heat-injection rate had a more significant effect than heat-injection temperature in promoting the decomposition of natural-gas hydrate.

Table 2. Area share of decomposition zone for different heat-injection rates.

Comparison Point	Heat-Injection Rate	Area Share (%)			
		Decomposing Zone	Non-Decomposition Zone	Decomposition Zone	Increase Extent
After 2 Days	$Q_{in} = 10 \text{ m}^3/\text{day}$		90.592	8.408	/
	$Q_{in} = 30 \text{ m}^3/\text{day}$		86.695	12.305	146.341
	$Q_{in} = 50 \text{ m}^3/\text{day}$		79.915	19.085	155.096
After 10 Days	$Q_{in} = 10 \text{ m}^3/\text{day}$	1	68.763	30.237	/
	$Q_{in} = 30 \text{ m}^3/\text{day}$		58.902	40.098	132.612
	$Q_{in} = 50 \text{ m}^3/\text{day}$		44.703	54.297	135.409
After 50 Days	$Q_{in} = 10 \text{ m}^3/\text{day}$		33.458	65.542	/
	$Q_{in} = 30 \text{ m}^3/\text{day}$		19.341	79.659	121.539
	$Q_{in} = 50 \text{ m}^3/\text{day}$		1.797	97.203	122.024

4. Conclusions

- (1) Final cumulative production was approximately equivalent for different heat-injection temperatures and heat-injection rates as there was sufficient injection heat to ensure complete decomposition of hydrate in reservoir. Cumulative production reached a maximum within fewer days for higher heat-injection temperature or heat-injection rate. Daily production for different heat-injection temperatures and heat-injection rates showed a similar pattern of variation, with daily production rising rapidly to a peak at the beginning, gradually decreasing to a certain value, then showing a certain magnitude of increase, and then decreasing slowly until the final daily gas production was 0 m³/day.
- (2) Temperature distribution and saturation distribution are introduced to characterize the decomposition characteristics of natural-gas hydrate in the process of heat-injection production. The temperature-distribution contours were similar for different heat-injection temperatures or different heat-injection rates, and the temperature-distribution-contours' sparsity could be seen as "sparse–dense–sparse" as the distance to the injection well increased. The high-temperature area became larger as the heat-injection rate increased. The saturation-distribution contours showed an outward convex trend along the injection-production direction with heat injection, and the outward convex trend was more obvious as heat-injection temperature and heat-injection rate increased.
- (3) The reservoir could be divided into three different areas—decomposition zone, decomposing zone, and non-decomposition zone—by the decomposition front, with the decomposition gas and water flowing rapidly away from the decomposition zone under certain pressure differences. Saturation had a steeply changing area i.e., the decomposition front occurred due to the rapid temperature increase in the instantaneous contact process of heat injection, and the temperature of the decomposition front was about 15–17 °C. With the increase in the heat-injection temperature, the decomposition front moved faster, the area share of decomposition zone increased, but the increase extent decreased. With the increase in the heat-injection rate, the decomposition front moved faster, the area share of decomposition zone increased, and the increase extent increased. The high heat-injection rate had a more significant effect than heat-injection temperature in promoting the decomposition of natural-gas hydrate.

Author Contributions: Conceptualization, Q.Y. and K.Z.; methodology, S.L.; software, Z.C.; validation, H.T. and Y.Y.; formal analysis, H.T.; investigation, K.Z. and Y.Y.; resources, Q.Y. and C.L.; data curation, K.Z. and C.L.; writing—original draft preparation, K.Z.; writing—review and editing, C.L.; visualization, Z.C., C.L. and H.T.; supervision, S.L.; project administration, K.Z.; funding acquisition, Q.Y. and S.L. All authors have read and agreed to the published version of the manuscript.

Funding: This project was carried out under the framework of National Natural Science Foundation of China (No. 51804078) and Maoming Municipal Science and Technology Project (No. 2020513), and was financially supported by the Foundation for Young Talents in Higher Education of Guangdong, China (No. 2019KQNCX084).

Data Availability Statement: No new data were created.

Conflicts of Interest: The authors declare no conflict of interest.

References

1. Collett, T.S. Energy resource potential of natural gas hydrate. *AAPG Bull.* **2002**, *86*, 1971–1992.
2. Li, D.; Zhang, L.; Guo, L.; Xiong, Y.; Liang, X. Microwave heating technique to exploit natural gas hydrate reservoir. *Spec. Oil Gas Reserv.* **2005**, *12*, 12.
3. Chejara, A.; Kvamme, B.; Vafaei, M.T.; Jemai, K. Simulations of long term methane hydrate dissociation by pressure reduction using an extended RetrasoCodeBright simulator. *Energy Convers. Manag.* **2013**, *68*, 313–323. [[CrossRef](#)]
4. Li, G.; Li, B.; Li, X.; Zhang, Y.; Wang, Y. Experimental and numerical studies on gas production from methane hydrate in porous media by depressurization in pilot-scale hydrate simulator. *Energy Fuel* **2012**, *26*, 6300–6310. [[CrossRef](#)]
5. Zhou, X.; Fan, S.; Liang, D. Advancement in research on replacement of CH₄ from hydrate with CO₂. *Chem. Ind. Eng. Prog.* **2006**, *25*, 524–527.
6. Moridis, G.J.; Collett, T.S.; Dallimore, S.R.; Satoh, T.; Hancock, S.; Weatherill, B. Numerical studies of gas production from several CH₄-hydrate zones at the Mallik Site, Mackenzie Delta, Canada. *J. Pet. Sci. Eng.* **2004**, *43*, 219–238. [[CrossRef](#)]
7. Uddin, M.; Wright, F.; Dallimore, S.; Coombe, D. Gas hydrate decompositions in Mallik hydrate bearing zones A, B, and C by depressurization: Effect of salinity and hydration number in hydrate decomposition. *J. Nat. Gas Sci. Eng.* **2014**, *21*, 40–63. [[CrossRef](#)]
8. McGuire, P. Recovery of gas from hydrate deposits using conventional technology. In Proceedings of the SPE Unconventional Gas Recovery Symposium, Pittsburgh, PA, USA, 16–18 May 1982.
9. Holder, G.D.; Angert, S. Simulation gas production from a reservoir containing both gas hydrate and free natural gas. In Proceedings of the Fall Technical Conference & Exhibition of the Society of Petroleum Engineers of Aime, San Francisco, CA, USA, 26–29 September 1982.
10. Kamath, V.A.; Godbole, S.P. Evaluation of hot-brine stimulation technique for gas production from natural gas hydrate. *J. Pet. Technol.* **1985**, *39*, 11. [[CrossRef](#)]
11. Sellm, M.S.; Sloan, E.D. Hydrate Decomposition in Sediment. *SPE Reserv. Eng.* **1990**, *5*, 245–251. [[CrossRef](#)]
12. Swinkels, W.; Drenth, R.J.J. Thermal Reservoir Simulation Model of Production from Naturally Occurring Gas Hydrate Accumulations. In Proceedings of the SPE Annual Technical Conference and Exhibition, Houston, TX, USA, 3–6 October 1999.
13. Moridis, G.J. Numerical studies of gas production from methane hydrates. *SPE J.* **2002**, *8*, 359–370. [[CrossRef](#)]
14. Moridis, G.; Collett, T. Strategies for Gas Production from Hydrate Accumulations under Various Geologic Conditions. In Proceedings of the TOUGH Symposium 2003, Berkeley, CA, USA, 12–14 May 2003; 2003.
15. Tang, L.G.; Feng, Z.P.; Shen, Z.Y.; Du, Y. Thermodynamic evaluation of natural gas hydrate production by thermal stimulation. *J. Eng. Thermophys.* **2007**, *28*, 1.
16. Du, Q.; Chen, Y.; Li, S.; Sun, J.; Jiang, L. Mathematical model for natural gas hydrate production by heat injection. *Pet. Explor. Dev.* **2007**, *34*, 1505–1507.
17. Hou, L.; Wu, Y.; Xu, J.; Sun, J. A study on the seepage model for the exploitation of natural gas hydrate by thermal excitation. *J. Xi'an Shiyou Univ. Nat. Sci. Ed.* **2008**, *23*, 44–45.
18. Li, M.; Fan, S. Thermal infection analysis on hot water flooding decomposition frontal brim of natural gas hydrate. *Acta Oceanol. Sin.* **2012**, *34*, 116–119.
19. Phirani, J.; Pitchumani, R.; Mohanty, K.K. History matching of hydrate formation and decomposition experiments in porous media. In Proceedings of the SPE Reservoir Simulation Symposium, The Woodlands, TX, USA, 2–4 February 2009.
20. Peng, Y.; Jin, G.; Su, Z.; Liu, L.; Liu, J.; Zhai, H. Sensitivity study on key geological parameters of gas hydrate production. *Adv. NR Energy* **2021**, *9*, 133–142.
21. Bai, Y.; Li, Q.; Li, X.; Du, Y. Simulation of natural gas hydrate reservoir extraction with lower volatile gas. *Chin. Sci. Bull.* **2008**, *53*, 2244–2250.
22. Zhao, Z. Thermodynamic analysis for the gas production from gas hydrate by heating. *China Min. Mag.* **2013**, *22*, 125–128.
23. Zhao, J.; Wang, J.; Liu, W.; Song, Y. Analysis of heat transfer effects on gas production from methane hydrate by thermal stimulation. *Int. J. Heat Mass Transf.* **2015**, *87*, 145–150. [[CrossRef](#)]
24. Keming, S.; Tingting, W.; Cheng, Z.; Huiyu, L. Patterns of Reservoir Deformation due to Thermal Decomposition of Natural Gas hydrate. *Spec. Oil Gas Reserv.* **2017**, *24*, 91–96.
25. Liu, Y.; Bai, Y.; Xia, Z.; Hou, J. Parameter optimization of depressurization to Hot Water Flooding in heterogeneous hydrate bearing layers based on the particle swarm optimization algorithm. *J. Nat. Gas Sci. Eng.* **2018**, *53*, 403–415. [[CrossRef](#)]
26. Liu, Y.; Hou, J.; Zhao, H.; Liu, X.; Xia, Z. Numerical simulation of simultaneous exploitation of geothermal energy and natural gas hydrate by water injection into a geothermal heat exchange well. *Renew. Sustain. Energy Rev.* **2019**, *109*, 467–481. [[CrossRef](#)]

27. Peng, H.; Guan, F. Experimental study and numerical analysis on one-dimensional production by heat injection of methane hydrate in porous media. *Sci. Technol. Eng.* **2020**, *20*, 10856–10863.
28. Xia, Z.; Wang, X.; Shi, F.; Guo, J. Study of production of class I hydrate reservoir by hot water flooding. *Mar. Geol. Quat. Geol.* **2020**, *40*, 158–164.
29. Sun, S.; Liang, S.; Liu, Y.; Liu, D.; Gao, M.; Tian, Y.; Wang, J. A review on shale oil and gas characteristics and molecular dynamics simulation for the fluid behavior in shale pore. *J. Mol. Liq.* **2023**, *376*, 121507. [[CrossRef](#)]
30. Vakhin, A.V.; Khelkhal, M.A.; Tajik, A.; Ignashev, N.E.; Krapivnitskaya, T.O.; Peskov, N.Y.; Glyavin, M.Y.; Bulanova, S.A.; Slavkina, O.V.; Schekoldin, K.A. Microwave Radiation Impact on Heavy Oil Upgrading from Carbonate Deposits in the Presence of Nano-Sized Magnetite. *Processes* **2021**, *9*, 2021. [[CrossRef](#)]
31. Yousif, M.H.; Sloan, E.D. Experimental and theoretical investigation of methane-gas-hydrate decomposition in porous media. *SPE Reserv. Eng.* **1991**, *6*, 69–76.
32. Sawyer, W.K.; Boyer, C.M., II; Frantz, J.H., Jr.; Yost, A.B., II. Comparative assessment of natural gas hydrate production models. In Proceedings of the SPE CERI Gas Technology Symposium, Calgary, AB, Canada, 3–5 April 2000.
33. Ahmadi, G.; Ji, C.; Smith, D.H. Production of natural gas from methane hydrate by a constant downhole pressure well. *Energy Convers. Manag.* **2007**, *48*, 2053–2068. [[CrossRef](#)]
34. Zhai, C.; Sun, K.; Xin, L.; Wang, T. Numerical Simulation Research of Deformation and Fracture of The Formation Near the Wellbore During the Heat Injection Exploitation of Natural Gas Hydrates. *J. Geomech.* **2017**, *23*, 821–828.
35. Fakcharoenphol, P.; Wu, Y.S. A Fully-Coupled Flow-Geomechanics Model for Fluid and Heat Flow in Geothermal Reservoirs. In Proceedings of the Geothermal Resources Council Annual Meeting, San Francisco, CA, USA, 26–29 June 2011.
36. Cheng, Y.; Shen, H.; Zhao, Y.; Zhang, J.; Xia, Y. Study on fluid-solid coupling of physical variation of gas hydrate reservoirs during natural gas development. *Acta Pet. Sin.* **2010**, *31*, 607–611.
37. Ji, C.; Ahmadi, G.; Smith, D.H. Natural gas production from hydrate decomposition by depressurization. *Chem. Eng. Sci.* **2001**, *56*, 5801–5814. [[CrossRef](#)]

Disclaimer/Publisher’s Note: The statements, opinions and data contained in all publications are solely those of the individual author(s) and contributor(s) and not of MDPI and/or the editor(s). MDPI and/or the editor(s) disclaim responsibility for any injury to people or property resulting from any ideas, methods, instructions or products referred to in the content.